Composites Communications 56 (2025) 102395

Contents lists available at ScienceDirect

Composites Communications

journal homepage: www.elsevier.com/locate/coco

Research article

Tensile damage analysis of composite structures based on 3D Hashin failure criteria and 2D higher-order structural theories

M. Petrolo *,[1], E. Tortorelli[2], S. Saputo[3], E. Carrera[4]

MUL² Lab, Department of Mechanical and Aerospace Engineering, Politecnico di Torino, Corso Duca degli Abruzzi 24, 10129 Torino, Italy

ARTICLE INFO

Keywords:
Composites
Damage
Hashin
CUF
FEM

ABSTRACT

This paper combines higher-order two-dimensional (2D) structural theories and Hashin 3D criteria for the progressive damage analysis of composite structures. The structural model is based on the Carrera Unified Formulation (CUF), which allows the implementation of any-order structural theory, and a layer-wise formulation is used. The current work employs first- to third-order Lagrange polynomials along the thickness of each ply. Numerical tests concern tensile loads and focus on a single element for verification and, then, on the stress–strain curves and damage distributions of center-notched and over-height tensile specimens. Convergence analyses are carried out, and the impact of increasing the scale of specimens on the computational costs is assessed. Comparisons with numerical and experimental results from the literature are carried out. The results show a good match with numerical references and experimental data. The use of higher-order 2D theories leads to lower computational overhead with no accuracy penalties. In fact, higher-order kinematics can detect 3D stress and strain fields without the necessity of employing refined solid meshes. Furthermore, increasing the specimen scale does not lead to higher computational costs.

1. Introduction

Fiber-reinforced composites are an important class of materials in the aerospace sector today due to their advantageous properties like high specific strength and stiffness [1]. However, analyzing progressive damage in fiber-reinforced composites is challenging due to the various failure modes that occur under applied loading conditions and their interactions. Failure modes are complex, and it is not straightforward to translate them into a numerical material model while maintaining the physics of damage progression and its impact on structural integrity. Therefore, the numerical modeling of progressive damage in composites is a highly active research area, as indicated by the substantial scientific literature produced over the past few decades [2,3].

Typically, computational models that simulate the progressive damage in fiber-reinforced composites are divided into discrete damage models (DDM) and continuum damage models (CDM). The first method provides physically accurate damage mechanisms and their interactions, considering the explicit geometrical representation of cracks within the structure. Still, it comes with a significant increase in computational workload. DDM techniques usually consider discontinuities across cracks within the finite element mesh. A common approach is the eXtended-Finite Element Method (x-FEM) [4,5]. Another technique for discrete modeling involves using cohesive models based on the Cohesive Zone Method (CZM). Discrete damage models based on cohesive interface elements have been applied to the progressive damage analysis of laminates under tensile loads and the interaction between matrix cracks and delamination [6,7].

An alternative approach to reduce computational costs is based on continuum damage mechanics (CDM). The cracks within the composite matrix are distributed throughout the volume of the finite element, and their effects are represented by damage parameters that influence the stiffness of the material point within the global structure [8]. However, the CDM approach shows a strong mesh dependency. To mitigate this problem, the crack-band theory is typically used, scaling the fracture energy with a characteristic length derived from the finite element's dimensions [9]. The first to apply the CDM to study the creep rupture of metals was Kachanov [10]. Some initial works on continuum damage

* Corresponding author.
E-mail addresses: marco.petrolo@polito.it (M. Petrolo), elisa.tortorelli@polito.it (E. Tortorelli), salvatore.saputo@polito.it (S. Saputo), erasmo.carrera@polito.it (E. Carrera).
[1] Associate Professor.
[2] PhD Student.
[3] Research Assistant.
[4] Professor of Aeronautics and Astronautics.

https://doi.org/10.1016/j.coco.2025.102395
Received 15 February 2025; Received in revised form 26 March 2025; Accepted 4 April 2025
Available online 19 April 2025

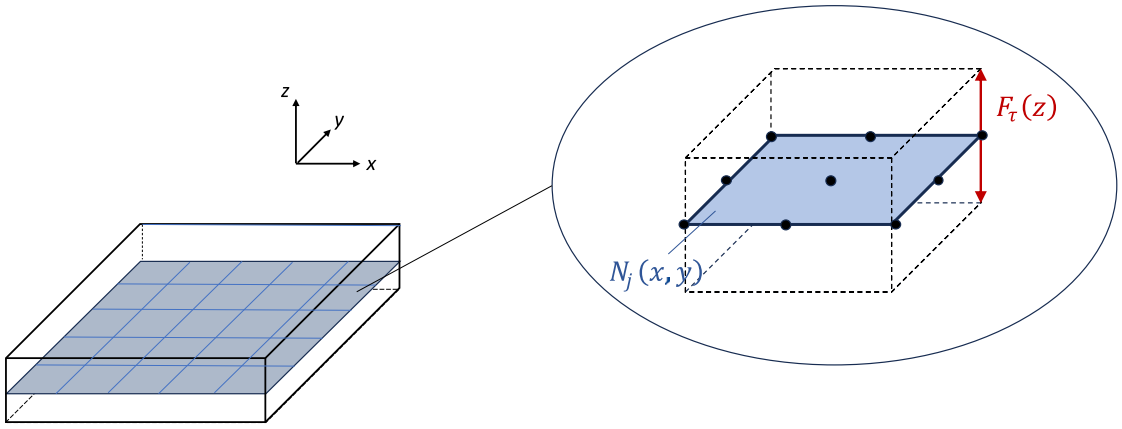

Fig. 1. Reference frame and Q9 elements.

modeling of composite laminates include the works of Matzenmiller et al. [11] and Ladaveze et al. [12]. Several recent studies employing continuum damage modeling have investigated various aspects of composite materials, ranging from the analysis of size effects in composite laminates [13], the notched behavior of composite laminates under tension [14], the progressive damage analysis of composite structures loaded in compression [15], and the impact analysis of composite plates [16].

In the continuum damage mechanics, the material degradation rules are based on the failure criteria to predict damage initiation, progressive failure properties, and ultimate failure strengths of composite laminates. Continuous efforts are underway to develop failure criteria to predict initial failure and microcracking in composite laminates. Examples of these criteria include the maximum stress, Hashin, Puck, Hoffman, Yamada–Sun, Tsai–Hill, and Tsai–Wu criteria [17–22]. Arruda et al. [23] introduced an innovative 2D orthotropic damage model based on the Tsai–Wu criterion capable of identifying significant failure mechanisms. In [24], a non-linear progressive damage model is presented, combining the Hashin and Matzenmiller–Lubliner–Taylor (MLT) failure criteria and applied to 3D woven composites. Other works adopt 3D Hashin failure criteria [25,26].

The computational costs of progressive damage analysis for composite structures can be extremely high, even with the relative efficiency of CDM models, especially for complex structures. This is often due to the necessity of refined, usually 3D, meshes to achieve an accurate stress field, which is crucial for the nonlinear material model. Various techniques have been suggested in the literature to enhance the computational efficiency of these analyses. A popular method is solid/shell coupling, where the global structure is composed of shell elements, with solid elements used only in regions where damage is likely to occur as in the global/local approach [27,28].

The current work focuses on the improvement of the computational efficiency by using the Carrera Unified Formulation (CUF) [29] with two-dimensional (2D) finite elements based on higher-order structural theories to obtain accurate 3D stress fields [30]. CUF capabilities in the progressive damage model have been shown in recent years by Nagaraj et al. [31,32] using CODAM2 [33] and a 2D Hashin failure criterion. Trombini et al. [34] combined the Hashin 3D orthotropic model with refined one-dimensional (1D) finite elements based CUF. The present work extends the development by considering the Hashin 3D orthotropic model and 2D finite elements. The Layer-Wise (LW) approach is used to model the through-the-thickness behavior of plates [35,36], where displacement field continuity is ensured at each ply interface [36]. LW is useful for progressive damage analyses as it improves the accuracy of transverse stresses, including interface continuity. This work extends previous research by integrating higher-order CUF-based LW theories with 3D Hashin failure criteria for progressive damage analysis underlying the capability of LW formulation based on the CUF to predict accurate 3D stress without requiring refined 3D meshes.

This paper is structured as follows: Section 2 describes CUF and finite element method for 2D models; Section 3 presents an overview of the continuum damage model and failure criteria. Numerical results are presented in Section 4. Then, the key conclusions of this study are summarized in Section 5.

2. Structural theories and finite elements formulation

The two-dimensional (2D) model adopted in this work is based on the Carrera Unified Formulation (CUF) [29]. CUF allows writing the unknown fields and relating governing equations of any 1D or 2D refined theory using fundamental nuclei (FN) [37], whose expressions do not depend on the assumptions used, such as type and order of the functions. Using the reference system shown in Fig. 1, the three-dimensional (3D) displacement field, $\boldsymbol{u}(x,y,z)$, can be expressed as a product between a 2D in-plane shape function, $N_i(x,y)$, and 1D expansion function $F_\tau(z)$,

$$\boldsymbol{u}(x,y,z) = F_\tau(z) N_i(x,y) \boldsymbol{u}_{\tau i}, \qquad \tau = 1,\dots,M \qquad i = 1,\dots,p \tag{1}$$

$F_\tau(z)$ are the expansion functions modeling the displacement field along the thickness and having "M" terms. $\boldsymbol{u}_{\tau i}$ is the nodal unknown vector. $N_i(x,y)$ are the 2D shape functions, and p is the number of nodes of each element. This work uses four- (Q4) and nide-node (Q9) elements. The choice of F_τ and its order is an input of the analysis and is usually done via a convergence analysis. F_τ defines the structural theory adopted. The modeling strategy of this paper is layer-wise (LW), i.e., the displacement variables are defined on each layer, and continuity is imposed at the interface. In the LW case, the displacement field becomes

$$\boldsymbol{u}^k(x,y,\zeta^k) = F_\tau^k(\zeta^k) \boldsymbol{u}_\tau^k(x,y), \qquad \tau = 1,\dots,M \tag{2}$$

k is the ply index and ζ^k is the thickness domain, [−1,1]. The current work uses the Lagrange expansions (LE); first- (LE1), second- (LE2), and third-order (LE3) polynomials are used. Further information on applying Lagrange polynomials as an expansion function for 2D plate modeling can be found in [29]. The 3D stress and strain components are grouped as follows:

$$\begin{aligned} \boldsymbol{\sigma} &= \{\sigma_{xx}, \sigma_{yy}, \sigma_{zz}, \sigma_{xy}, \sigma_{xx}, \sigma_{yz}\}^T \\ \boldsymbol{\epsilon} &= \{\epsilon_{xx}, \epsilon_{yy}, \epsilon_{zz}, \epsilon_{xy}, \epsilon_{xz}, \epsilon_{yz}\}^T \end{aligned} \tag{3}$$

The linear strain–displacement relation is considered,

$$\boldsymbol{\epsilon} = \mathbf{B}\boldsymbol{u} \tag{4}$$

where the linear differential operator **B** is

$$\boldsymbol{B} = \begin{bmatrix} \partial_x & 0 & 0 \\ 0 & \partial_y & 0 \\ 0 & 0 & \partial_z \\ \partial_y & \partial_x & 0 \\ \partial_z & 0 & \partial_x \\ 0 & \partial_z & \partial_y \end{bmatrix} \tag{5}$$

The constitutive relation considering the damaged state can be written as follows:

$$\boldsymbol{\sigma} = \mathbf{C}^{sec}\epsilon \tag{6}$$

$\mathbf{C}^{sec}$ is the secant material stiffness matrix. The equations are solved using explicit time integration techniques and the central difference scheme. More details on implementing the explicit scheme in CUF can be found in [31].

3. Damage model

This paper adopts the 3D Hashin criteria for matrix and fiber tensile failures [38]. The fiber damage initiation occurs when failure index $F_{ft} \geq 1$, with

$$F_{ft} = \left(\frac{\sigma_{11}}{X_T}\right)^2 + \alpha_f \left[\left(\frac{\sigma_{12}}{S_{12}}\right)^2 + \left(\frac{\sigma_{13}}{S_{13}}\right)^2\right] \tag{7}$$

X_T is the fiber tensile strength, and S_{12} and S_{13} are the shear strengths. α_f is the interaction coefficient for fibers and, unless otherwise stated, is set equal to zero. A more comprehensive discussion on this parameter is added in the result section. Similarly, $F_{mt} \geq 1$ for the matrix damage initiation along the transverse direction, with

$$F_{mt} = \left(\frac{\sigma_{22}+\sigma_{33}}{Y_T}\right)^2 + \frac{1}{S_{23}^2}(\sigma_{23}^2 - \sigma_{22}\sigma_{33}) + \left(\frac{\sigma_{12}}{S_{12}}\right)^2 + \left(\frac{\sigma_{13}}{S_{13}}\right)^2 \tag{8}$$

Y_T is the matrix tensile strength, and S_{23} is the shear strength. The damage progression criteria exploit equivalent tensile displacements, δ_{eq}^{ft} and δ_{eq}^{mt}, for fibers and matrix, respectively,

$$\delta_{eq}^{ft} = l_c\sqrt{\langle\epsilon_{11}\rangle^2 + \epsilon_{12}^2 + \epsilon_{13}^2} \tag{9}$$

$$\delta_{eq}^{mt} = l_c\sqrt{\langle\epsilon_{22}\rangle^2 + \langle\epsilon_{33}\rangle^2 + \epsilon_{12}^2 + \epsilon_{23}^2 + \epsilon_{13}^2} \tag{10}$$

$\langle\cdot\rangle$ is the Mcaulay bracket, l_C is the characteristic length set equal to the cubic root of the Gauss point volume, $l_C = (V_{GP})^{1/3}$. The Gauss point volume is the portion of the element volume associated with each Gauss point. For instance, with one Gauss point, the Gauss point volume equals the entire element volume. With two Gauss points, each Gauss point volume is half of the element volume. Furthermore, the characteristic length relates the displacement to the equivalent strain as $\delta_{eq} = l_c\epsilon_{eq}$. The corresponding equivalent stresses in the longitudinal and transverse directions are

$$\sigma_{eq}^{ft} = \frac{l_c(\langle\sigma_{11}\rangle\langle\epsilon_{11}\rangle + \sigma_{12}\epsilon_{12} + \sigma_{13}\epsilon_{13})}{\delta_{eq}^{ft}} \tag{11}$$

$$\sigma_{eq}^{mt} = \frac{l_c(\langle\sigma_{22}\rangle\langle\epsilon_{22}\rangle + \langle\sigma_{33}\rangle\langle\epsilon_{33}\rangle + \sigma_{12}\epsilon_{12} + \sigma_{23}\epsilon_{23} + \sigma_{13}\epsilon_{13})}{\delta_{eq}^{mt}} \tag{12}$$

Fig. 2 shows the constitutive equivalent stress–displacement relation in which the ultimate displacement corresponds to the damage saturation,

$$\delta_{eq}^{u,f} = \frac{2G_f}{X_T} \tag{13}$$

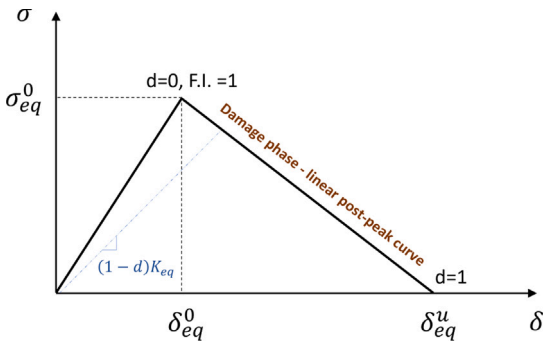

Fig. 2. Constitutive equivalent stress–displacement relation.

$$\delta_{eq}^{u,m} = \frac{2G_m}{T} \tag{14}$$

G_f and G_m are the fracture energies in longitudinal and transverse directions, respectively; T is the peak value of the equivalent transverse stress when the damage occurs, $T = \sigma_{eq}^{mt}\big|_{F_m=1}$. The equivalent stress and displacement at the damage initiation are necessary to define the damage evolution. In this paper, a parameter, d, is used as follows:

$$d = \frac{\delta_{eq}^u(\delta_{eq} - \delta_{eq}^0)}{\delta_{eq}(\delta_{eq}^u - \delta_{eq}^0)} \tag{15}$$

$\delta_{eq}^0 = \delta_{eq}\big|_{F=1}$ is the equivalent displacement at the damage initiation. The stiffness matrix in the damaged state, $\boldsymbol{C}^{dam}$, is

$$\boldsymbol{C^{dam}} = \frac{1}{\Delta}\begin{bmatrix} C_{11} & C_{12} & C_{13} & 0 & 0 & 0 \\ C_{21} & C_{22} & C_{23} & 0 & 0 & 0 \\ C_{31} & C_{32} & C_{33} & 0 & 0 & 0 \\ 0 & 0 & 0 & C_{44} & 0 & 0 \\ 0 & 0 & 0 & 0 & C_{55} & 0 \\ 0 & 0 & 0 & 0 & 0 & C_{66} \end{bmatrix} \tag{16}$$

$$\Delta = 1 - (1-d_f)(1-d_m)\nu_{12}\nu_{21} - (1-d_m)\nu_{23}\nu_{32} - (1-d_f)\nu_{13}\nu_{31} - 2(1-d_f)(1-d_m)\nu_{21}\nu_{32}\nu_{13} \tag{17}$$

The damage parameters d_f and d_m refer to fiber and matrix, respectively,

$$d_f = 1 - (1-d_{ft})(1-d_{fc}) \tag{18}$$

$$d_m = 1 - (1-d_{mt})(1-d_{fc}) \tag{19}$$

d_{ft} and d_{mt} refer to fiber and matrix traction, d_{fc} and d_{mc} to fiber and matrix compression. The matrix components are defined as

$$C_{11} = [1-(1-d_m)\nu_{23}\nu_{32}](1-d_f)E_1 \quad C_{12} = (1-d_f)(1-d_m)(\nu_{21}+\nu_{23}\nu_{31})E_1$$

$$C_{22} = [1-(1-d_f)\nu_{31}\nu_{13}](1-d_m)E_2 \quad C_{13} = (1-d_f)(\nu_{31}+(1-d_m)\nu_{21}\nu_{32})E_1$$

$$C_{33} = [1-(1-d_f)(1-d_m)\nu_{21}\nu_{12}]E_3 \quad C_{23} = (1-d_m)(\nu_{32}+(1-d_f)\nu_{12}\nu_{31})E_2$$

$$C_{44} = \Delta(1-d_f)(1-d_m)G_{12} \qquad C_{55} = \Delta G_{23}$$

$$C_{66} = \Delta G_{13} \tag{20}$$

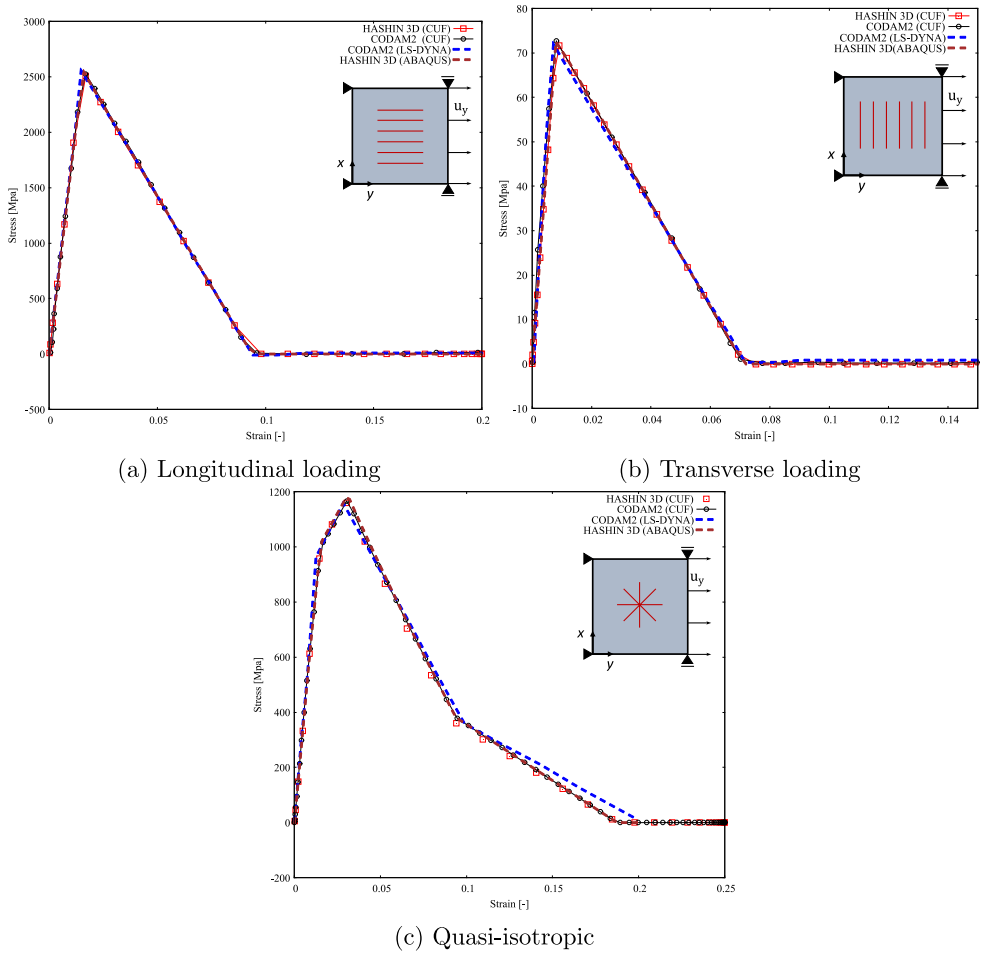

(a) Longitudinal loading

(b) Transverse loading

(c) Quasi-isotropic

Fig. 3. Stress–strain response of the single element under uni-axial traction.

The constitutive elastic stress–strain relation can be written as

$$\boldsymbol{\sigma} = \boldsymbol{C}^{dam}\boldsymbol{\epsilon} \tag{21}$$

More information about damage evolution parameters can be found in [31].

4. Numerical results

This section presents three numerical cases of tensile loading taken from the literature. The aim is to evaluate the accuracy and efficiency of the 3D Hashin damage model combined with 2D CUF theories when compared with the CODAM2 damage model, 2D Hashin criteria, experimental results, and Abaqus analyses.

4.1. Single element

The first numerical case considers a single element of 1 mm × 1 mm to verify the damage model. The material system used is IM7/8552 carbon fiber reinforced polymer (CFRP) with a ply thickness of 0.125 mm; see Table 1. The structural model is a Q4 with the ply thickness kinematics modeled using LE1 as in [31] with three loading cases. The first case consists of the uni-axial traction in the longitudinal direction with the fibers aligned to the y-direction. The second case consists of the loading in the transverse direction with respect to the fiber, i.e., fibers perpendicular to the y-direction. The last numerical example considers a quasi-isotropic $[90/45/0/-45]_{2s}$ laminate. Stress–strain curves are shown in Fig. 3 with results from four models: Hashin 3D and CUF; CODAM 2 and CUF taken from [31]; CODAM 2 and LS-Dyna taken from [14]; and Hashin 3D with Abaqus continuum shell elements. Table 2 reports equivalent strains and stresses at damage initiation (ϵ^0_{eq} and σ^0_{eq}) and the ultimate equivalent strain (ϵ^u_{eq}). Based on the results obtained for the verification test of the single element, the following considerations are made:

1. The peak stresses predicted by the present model match the fiber and matrix material strengths, respectively. Once the maximum peak value has been reached, the load capacity decreases linearly until the damage saturation strain is reached.
2. For all three cases, the four modeling approaches provide very similar curves.

4.2. Center-notched specimen

The second numerical case considers a center-notched specimen under tension loading and based on [14], where size effects were investigated. In this work, the notch length is C=25.4 mm, the gauge width is W=127 mm, and the gauge length is L=508 mm. The boundary conditions and geometry of the specimen are shown in Fig. 4, where the specimen is clamped at one edge and a displacement along y-direction is applied at the free edge. The material system used in each case is IM7/8552 CFRP as in Table 1. The ply stacking sequence is $[45/90/-45/0]_{4s}$ with a ply thickness of 0.125 mm. The results are compared with models taken from [14]; namely, LS-Dyna employing the CODAM2 and a Ladeveze-based damage model from Abaqus (ABQ-DLR), with the fiber damage evolution by an exponential softening law in [14]. Furthermore, experimental results retrieved from [39] are used for validation.

Table 1
Material properties of IM7/8552.

E_1 (GPa)	E_2 (GPa)	E_3 (GPa)	G_{12} (GPa)	G_{13} (GPa)	G_{23} (GPa)	ν_{12}	ν_{13}	ν_{23}
150.0	11.0	11.0	5.8	5.8	2.9	0.34	0.34	0.48
X_T (MPa)	X_C (MPa)	Y_T (MPa)	Y_C (MPa)	S_{12} (MPa)	G_1^T (kJ/m^2)	G_2^T (kJ/m^2)	G_1^C (kJ/m^2)	G_2^C (kJ/m^2)
2560	11 690	73	250	90	120	2.6	80.0	4.2

Table 2
Comparison of equivalent strain at damage initiation, strain at damage saturation and peak stress for the single element,$[90/45/0/-45]_{2s}$.

	Hashin 3D/CUF	CODAM2/CUF	CODAM2/LS-Dyna	HASHIN 3D/Abaqus
ϵ_{eq}^0	0.028	0.028	0.027	0.027
ϵ_{eq}^u	0.185	0.186	0.199	0.185
σ_{eq}^0 (MPa)	1166.3	1166.2	1165.9	1165.8

Table 3
DOF and equivalent strains and stresses at damage initiation for the center-notched specimen.

	74Q9-LE1	88Q9-LE1	132Q9-LE1	132Q9-LE2	132Q9-LE3	184Q9-LE1	Exp. min	Exp.max
DOF	33 660	39 600	61 380	120 900	180 420	79 200		
ϵ_{eq}^0	0.675	0.643	0.548	0.555	0.563	0.526		
σ_{eq}^0 (MPa)	407.6	392.1	334.4	341.8	342.5	323.2	335.4	345.2

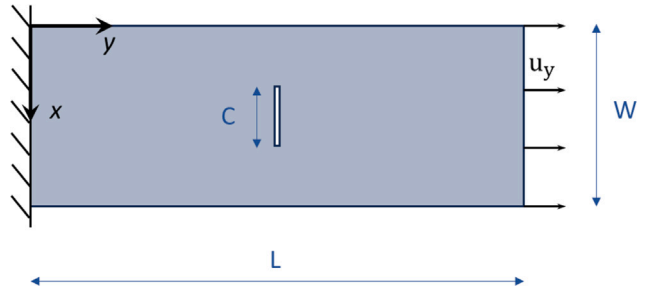

Fig. 4. Boundary conditions and geometry of the center-botched specimen under tension.

Table 4
Dimensions (mm) of notch and specimen for different scales.

Scale	C	W	L
1	3.2	15.9	63.5
2	6.4	31.8	127.0
4	12.7	63.5	254.0
8	25.4	127.0	508.0
16	50.8	254.0	508.0

Table 5
Peak strength values and percentage errors respect to experimental value for different scales.

Scale	Model	Peak strength (MPa)	Error (%)
1	Experiments	590	–
	CODAM2-CUF	598	1.4
	ABQ-DLR	650	10.2
	HASHIN 3D-CUF	611	3.6
2	Experiments	525	–
	CODAM2-CUF	520	−0.9
	ABQ-DLR	530	0.9
	HASHIN 3D-CUF	524	−0.2
4	Experiments	452	–
	CODAM2-CUF	430	−4.9
	ABQ-DLR	430	−4.9
	HASHIN 3D-CUF	459	1.5
8	Experiments	350	–
	CODAM2-CUF	343	−2.0
	ABQ-DLR	330	−5.7
	HASHIN 3D-CUF	350	0.0
16	Experiments	260	–
	CODAM2-CUF	279	7.3
	ABQ-DLR	240	−7.7
	HASHIN 3D-CUF	281	8.1

Fig. 5 shows the stress–strain curves using the 3D Hashin criteria and showcasing the impact of mesh refinement with Q9 elements increasing from 74 to 184. Furthermore, the expansion order along the thickness also increases from linear to cubic. These results are compared to the maximum and minimum strength values from experimental results [39]. Table 3 shows the number of DOF of each model and the equivalent strain and stress at damage initiation. Fig. 6 shows a comparison with CODAM2 results from CUF [31] and LS-Dyna [14]. Fig. 7 shows the stress–strain curve of the specimen with 132 Q9 LE1 for $\alpha_f = 0$ and $\alpha_f = 1$.

The last set of results considers different specimen scales to investigate the influence of the dimensions on the computational cost. The dimensions of the specimen for various scales are reported in Table 4 where C corresponds to the notch length, W to the specimen width and L to the specimen length, and the 132 Q9 LE1 was used. Fig. 8 shows the maximum peak stress for different scales, models [14,31] and experiments [39]. Table 5 shows the error with respect to the experimental data of all models. Fig. 9 shows the DOF employed for each scale and model alongside the computational time utilized. The latter is normalized with respect to the computational time of scale 1 for each approach. The DOF difference between the present model and that employed in [31] is due to the modeling approach in the latter in which plies of the same orientation were combined with a single LE 1.

The results suggest that:

1. The Hashin 3D failure model provides results similar to CODAM2, although closer to the experimental results. Overall, the new approach's accuracy is comparable to the other models. In three scales out of five, the present approach has a lower error.
2. From 132 Q9 onwards, the peak stress remains in the experimental range except when LE1 is used. The latter has a linear distribution of displacements in each layer, leading to constant transverse stress distributions. Depending on the problem characteristics, e.g., thickness, orthotropic ratio, stacking sequence, and boundary conditions, such a linear distribution may not be enough for reliable modeling, as shown in previous works by the authors [37].

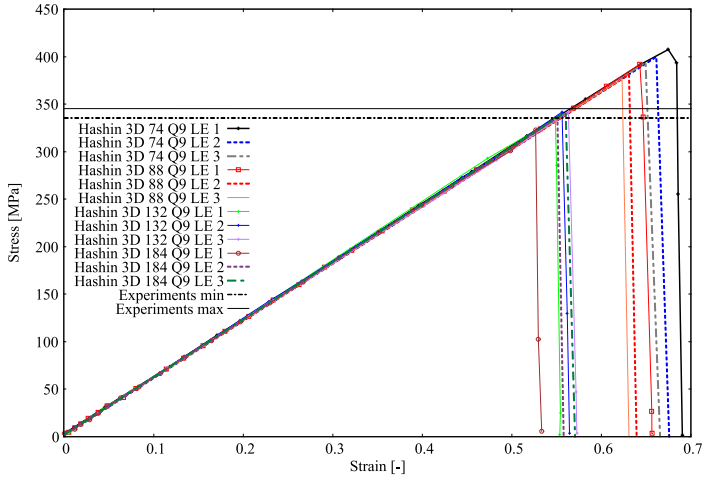

Fig. 5. Mesh and structural theory convergence for the stress–strain curve of center-notched specimen.

Table 6
Comparison of the pin opening displacement at damage initiation and the first peak force for the OCT with percentage error with respect to the experimental F_{max}.

	Hashin 3D-LE1	Hashin 3D-LE2	Hashin 3D-LE3	CODAM2-LE1	Experiments
POD (mm)	1.142	1.192	1.233	1.142	0.888
F_{max} (kN)	12.08	12.39	13.09	12.11	9.72
Error F_{max} (%)	24.3	27.5	34.7	24.6	–

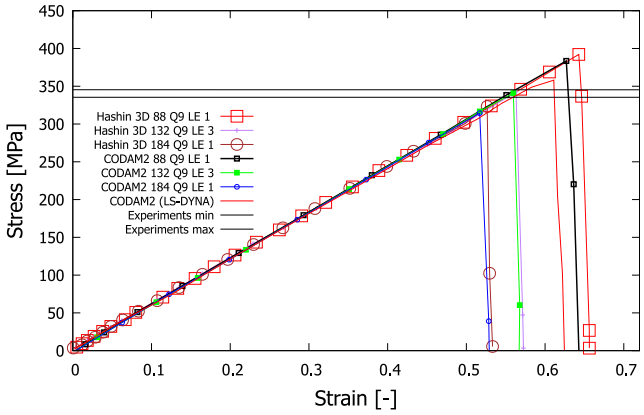

Fig. 6. Stress–strain curves of center-notched specimen using Hashin 3D and CODAM2.

3. In Fig. 7, the stress–strain curves with and without the shear stress contribution agree, showing that the shear effect on fibers can be negligible.
4. The computational cost of CUF models is less affected by the specimen size than the standard finite element approach as demonstrated in 9. This is due to the possibility of using coarser meshes and higher-order kinematics over the thickness, as shown in a previous work [31].

4.3. Over-height compact tension test

The last numerical case refers to focuses on an over-height compact tension (OCT) with a ply sequence of $[90/45/0/-45]_{4s}$. The geometry and boundary conditions are shown in Fig. 10(a) and refer to the work [31]. Each pin is opened with a gradual displacement of up to 1 mm. The results are compared with experimental results from [40] obtained using the Digital Image Correlation (DIC) technique. The mesh has 392 Q9 as in [31]. The expansion order goes from linear (LE1) to cubic (LE3) along the thickness.

Fig. 11 shows the force–displacement curves from the current Hashin 3D compared with CODAM2 and experimental results. Table 6 reports the Pin Opening Displacement (POD) at the damage initiation point and the maximum forces and percentage errors. As for the previous test case, a comparison between $\alpha_f = 0$ and $\alpha_f = 1$ is shown in Fig. 12, and similar results were obtained. Fig. 13 shows the distribution of damage considering matrix and fiber damages at the peak stress. CUF was used for both Hashin 3D and CODAM2 with 392 Q9; furthermore, results from CODAM2 with LS-DYNA and the ABQ-DLR model based on the Ladeveze damage model were added.

The results highlight the following:

1. From the stress–strain curves in Fig. 11, it is evident that a discrepancy exists between the initiation of damage as predicted by the LE models and the experimental results, which can be attributed to the absence of delamination modeling in the adopted simulation.
2. The damage initiation of Hashin 3D-CUF and CODAM2-CUF occurs at the same POD of 1.142 mm, as listed in Table 6, showing a similar curve for both damage models. LE models

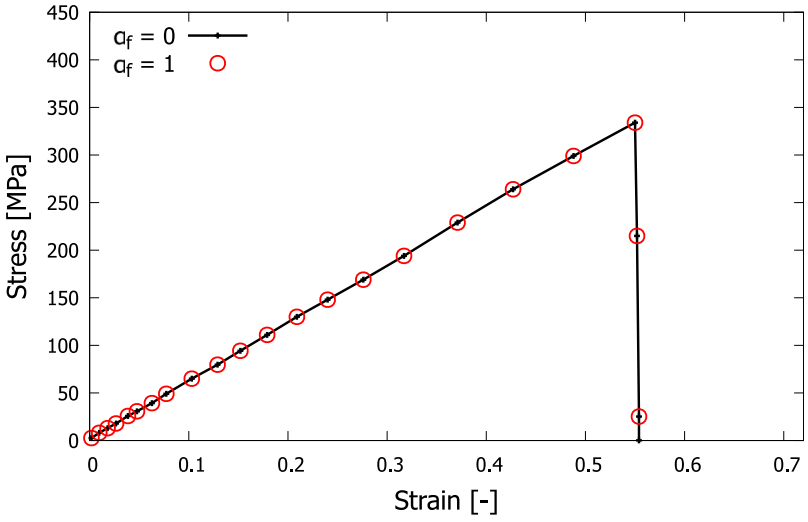

Fig. 7. The stress–strain curve of center-notched specimen, 132 Q9 LE1, $\alpha_f = 0$ and $\alpha_f = 1$.

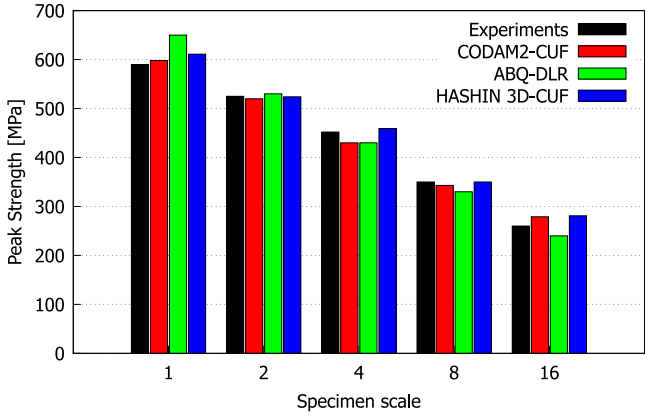

Fig. 8. Comparison of maximum peak stress obtained for various scales and using different models for the center-notched specimen.

have higher peaks than experimental results, possibly due to the absence of delamination modeling in the models adopted in this paper. In [41], CUF was used for delamination problems with a far better correlation with experimental results. On the other hand, LE1 has a displacement field quite similar to those of the other two numerical models from the literature, and thus, the match is closer.

3. The numerical oscillations in the CUF models in the post-peak curve are due to the absence of numerical damping and employment of fully integrated second-order elements Q9. The numerical models have smooth curves, but the experimental ones do not. As in [40], such behavior can stem from several factors, e.g., the heterogeneous nature of the fiber failure in the laminate, manufacturing defects, and interaction of failure mechanism, including splitting and delamination.
4. The distribution of damage shown in Fig. 13 suggests that at the same POD of 1.5 mm, a larger area near the crack begins to damage earlier for Hashin 3D rather than CODAM2.

5. Conclusions

This paper has discussed 2D high-order structural theories for the progressive damage analysis of composite structures. The focus is on combining layer-wise plate finite elements and Hashin 3D criteria. Starting from the CUF structural model and integrating failure criteria can describe the damage behavior of composite structures. The proposed approach's accuracy and computational efficiency have been assessed with numerical and experimental results from the literature. The numerical cases have focused on tensile loads on notched and over-height compact specimens. The following main conclusions may be drawn:

- Overall, the model proposed matches the results from the other approaches and offers a significant improvement in computational efficiency if compared to 3D models.
- The use of higher-order theories alleviates the need for mesh refinement and allows using the same meshes as the specimen scale increases. 2D elements have less severe aspect ratio constraints than 3D, and using higher-order kinematics can match the accuracy of solid elements.
- The use of Hashin 3D has led to larger damage areas if compared to CODAM2.
- The implementation of other failure mechanisms with the numerical model, e.g., delamination, is of paramount importance to match the experimental results.

Future work should concern the modeling of compressive behavior and delamination. Furthermore, multiscale models may also be used to evaluate the propagation of damage at the microscopic level.

CRediT authorship contribution statement

M. Petrolo: Writing – review & editing, Supervision, Methodology, Investigation, Funding acquisition, Formal analysis, Data curation, Conceptualization. **E. Tortorelli:** Writing – original draft, Validation, Investigation, Data curation. **S. Saputo:** Supervision, Investigation, Formal analysis, Data curation, Conceptualization. **E. Carrera:** Writing – review & editing, Supervision, Methodology, Investigation, Funding acquisition, Conceptualization.

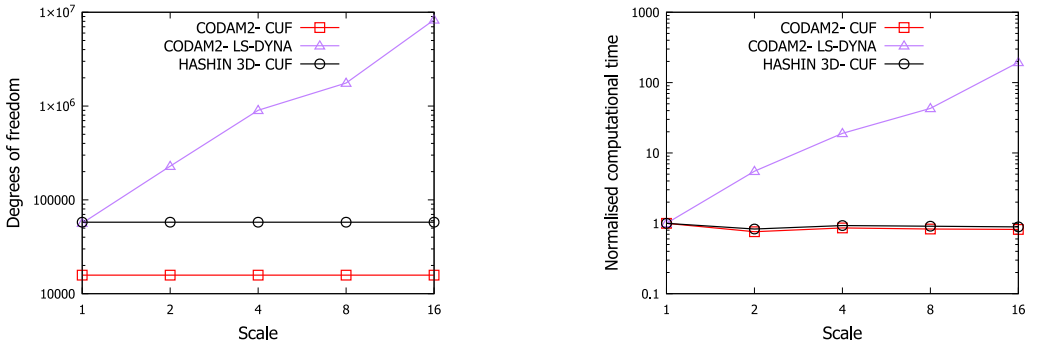

Fig. 9. Comparison for various scales and different numerical approaches of (a) DOF and (b) normalized computational time.

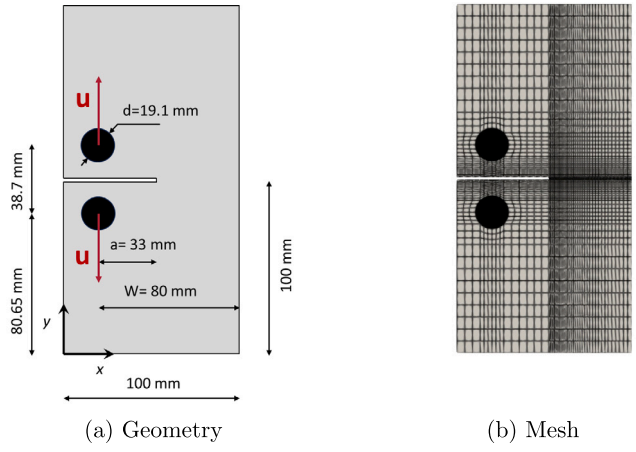

Fig. 10. Geometry, boundary conditions, and mesh of the OCT case.

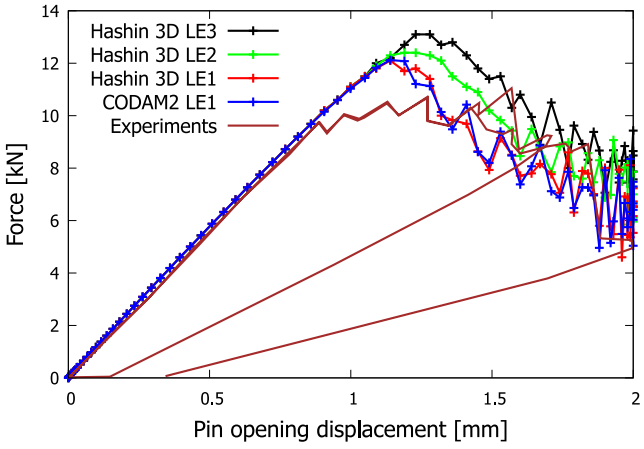

Fig. 11. Force–displacement curve of the OCT.

Declaration of competing interest

The authors declare that they have no known competing financial interests or personal relationships that could have appeared to influence the work reported in this paper.

Acknowledgments

This work was partially financed by the European Union - NextGenerationEU (National Sustainable Mobility Center CN00000023, Italian Ministry of University and Research Decree n. 1033 - 17/06/2022, Spoke 11 - Innovative Materials & Lightweighting). The opinions expressed are those of the authors only and should not be considered as representative of the European Union or the European Commission's official position. Neither the European Union nor the European Commission can be held responsible for them.

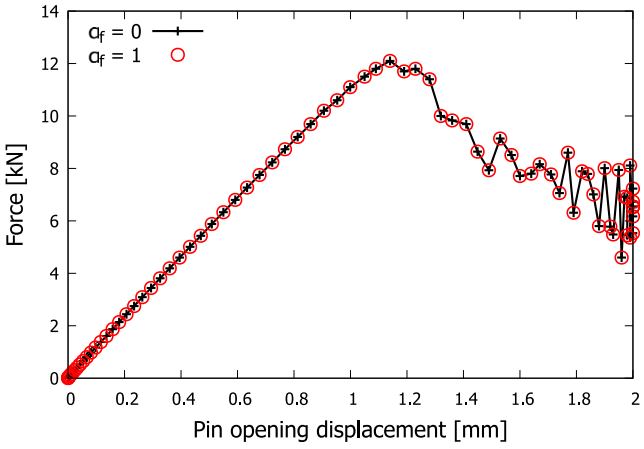

Fig. 12. Force–displacement curve of the OCT with $\alpha_f = 0$ and $\alpha_f = 1$.

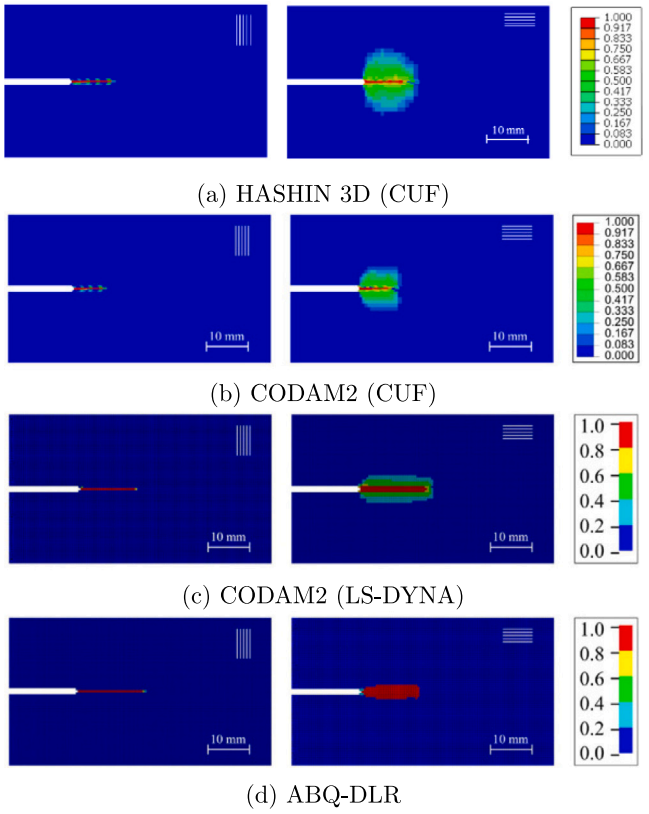

Fig. 13. Distribution of damage in the OCT case at POD=1.5 (mm) in the 90° ply corresponding to the matrix damage (right) and in the 0° ply corresponding to the fiber damage (left).

Data availability

Data will be made available on request.

References

[1] A.A. Baker, Composite Materials for Aircraft Structures, AIAA, 2004.

[2] A.C. Orifici, I. Herszberg, R.S. Thomson, Review of methodologies for composite material modelling incorporating failure, Compos. Struct. 86 (1) (2008) 194–210, Fourteenth International Conference on Composite Structures.

[3] C. Galiotis, A. Paipetis, Interfacial damage modelling of composites, in: C. Soutis, P.W.R. Beaumont (Eds.), Multi-Scale Modelling of Composite Material Systems, in: Woodhead Publishing Series in Composites Science and Engineering, Woodhead Publishing, 2005, pp. 33–64.

[4] E. Rivas, M. Parchei-Esfahani, R. Gracie, A two-dimensional extended finite element method model of discrete fracture networks, Internat. J. Numer. Methods Engrg. 117 (13) (2019) 1263–1282.

[5] M.J. Swindeman, E.V. Iarve, R.A. Brockman, D.H. Mollenhauer, S.R. Hallett, Strength prediction in open hole composite laminates by using discrete damage modeling, AIAA J. 51 (4) (2013) 936–945.

[6] S.R. Hallett, W. Jiang, B. Khan, M.R. Wisnom, Modelling the interaction between matrix cracks and delamination damage in scaled quasi-isotropic specimens, Compos. Sci. Technol. 68 (1) (2008) 80–89.

[7] C. Yao, Q.H. Jiang, J.F. Shao, C.B. Zhou, A discrete approach for modeling damage and failure in anisotropic cohesive brittle materials, Eng. Fract. Mech. 155 (2016) 102–118.

[8] K.V. Williams, R. Vaziri, A. Poursartip, A physically based continuum damage mechanics model for thin laminated composite structures, Int. J. Solids Struct. 40 (9) (2003) 2267–2300.

[9] Z.P. Bažant, B.H. Oh, Crack band theory for fracture of concrete, Matériaux et Constr. 16 (1983) 155–177.

[10] L.M. Kachanov, Time to failure under creep condition, Izv. Akad. Nauk. SSSR, Tech. Nauk. (8) (1958) 26–31.

[11] A.L.J.T.R. Matzenmiller, J. Lubliner, R.L. Taylor, A constitutive model for anisotropic damage in fiber-composites, Mech. Mater. 20 (2) (1995) 125–152.

[12] P. Ladeveze, E. LeDantec, Damage modelling of the elementary ply for laminated composites, Compos. Sci. Technol. 43 (3) (1992) 257–267.

[13] P.P. Camanho, P. Maimí, C.G. Dávila, Prediction of size effects in notched laminates using continuum damage mechanics, Compos. Sci. Technol. 67 (13) (2007) 2715–2727.

[14] J. Reiner, T. Feser, D. Schueler, M. Waimer, R. Vaziri, Comparison of two progressive damage models for studying the notched behavior of composite laminates under tension, Compos. Struct. 207 (2019) 385–396.

[15] Z.C. Su, T.E. Tay, M. Ridha, B.Y. Chen, Progressive damage modeling of open-hole composite laminates under compression, Compos. Struct. 122 (2015) 507–517.

[16] E.H. Kim, M.S. Rim, I. Lee, T.K. Hwang, Composite damage model based on continuum damage mechanics and low velocity impact analysis of composite plates, Compos. Struct. 95 (2013) 123–134.

[17] S.W. Tsai, E.M. Wu, A general theory of strength for anisotropic materials, J. Compos. Mater. 5 (1) (1971) 58–80.

[18] X. Li, D. Ma, H. Liu, W. Tan, X. Gong, C. Zhang, Y. Li, Assessment of failure criteria and damage evolution methods for composite laminates under low-velocity impact, Compos. Struct. 207 (2019) 727–739.

[19] O. Hoffman, The brittle strength of orthotropic materials, J. Compos. Mater. 1 (2) (1967) 200–206.

[20] A. Rotem, Z. Hashin, Failure modes of angle ply laminates, J. Compos. Mater. 9 (2) (1975) 191–206.

[21] R. Narayanaswami, H.M. Adelman, Evaluation of the tensor polynomial and Hoffman strength theories for composite materials, J. Compos. Mater. 11 (4) (1977) 366–377.

[22] Z. Hashin, Fatigue failure criteria for unidirectional fiber composites, J. Appl. Mech 47 (4) (1980) 329–334.

[23] M.R.T. Arruda, L. Almeida-Fernandes, L. Castro, J.R. Correia, Tsai–Wu based orthotropic damage model, Compos. Part C: Open Access 4 (2021) 100122.

[24] K.C. Warren, R.A. Lopez-Anido, S.S. Vel, H.H. Bayraktar, Progressive failure analysis of three-dimensional woven carbon composites in single-bolt, double-shear bearing, Compos. Part B: Eng. 84 (2016) 266–276.

[25] C. Hühne, A.K. Zerbst, G. Kuhlmann, C. Steenbock, R. Rolfes, Progressive damage analysis of composite bolted joints with liquid shim layers using constant and continuous degradation models, Compos. Struct. 92 (2) (2010) 189–200.

[26] B. Mandal, A. Chakrabarti, Simulating progressive damage of notched composite laminates with various lamination schemes, Int. J. Appl. Mech. Eng. 22 (2) (2017) 333–347.

[27] X.C. Sun, S.R. Hallett, Barely visible impact damage in scaled composite laminates: Experiments and numerical simulations, Int. J. Impact Eng. 109 (2017) 178–195.

[28] M. Akterskaia, E. Jansen, S.R. Hallett, P.M. Weaver, R. Rolfes, Progressive failure analysis using global-local coupling including intralaminar failure and debonding, AIAA J. 57 (7) (2019) 3078–3089.

[29] E. Carrera, M. Cinefra, M. Petrolo, E. Zappino, Finite Element Analysis of Structures Through Unified Formulation, John Wiley & Sons, 2014.

[30] A.G. de Miguel, I. Kaleel, M.H. Nagaraj, A. Pagani, M. Petrolo, E. Carrera, Accurate evaluation of failure indices of composite layered structures via various FE models, Compos. Sci. Technol. 167 (2018) 174–189.

[31] M.H. Nagaraj, J. Reiner, R. Vaziri, E. Carrera, M. Petrolo, Progressive damage analysis of composite structures using higher-order layer-wise elements, Compos. Part B: Eng. 190 (2020) 107921.

[32] M.H. Nagaraj, J. Reiner, R. Vaziri, E. Carrera, M. Petrolo, Compressive damage modeling of fiber-reinforced composite laminates using 2D higher-order layer-wise models, Compos. Part B: Eng. 215 (2021) 108753.

[33] K.V. Williams, R. Vaziri, A. Poursartip, A physically based continuum damage mechanics model for thin laminated composite structures, Int. J. Solids Struct. 40 (9) (2003) 2267–2300.

[34] M. Trombini, M. Enea, M.R.T. Arruda, A. Pagani, M. Petrolo, E. Carrera, 1D higher-order theories for quasi-static progressive failure analysis of composites based on a full 3D hashin orthotropic damage model, Compos. Part B: Eng. 270 (2024) 111120.

[35] E. Carrera, V.V. Zozulya, Carrera unified formulation (CUF) for the composite plates and shells of revolution. Layer-wise models, Compos. Struct. 334 (2024) 117936.

[36] A. Pagani, E. Carrera, R. Augello, D. Scano, Use of Lagrange polynomials to build refined theories for laminated beams, plates and shells, Compos. Struct. 276 (2021) 114505.

[37] D. Scano, E. Carrera, M. Petrolo, Use of the 3D equilibrium equations in the free-edge analyses for laminated structures with the variable kinematics approach, Aerotec. Missili Spaz. 103 (2024) 179–195, http://dx.doi.org/10.1007/s42496-023-00177-2.

[38] Y. Zhang, W. Van Paepegem, W. De Corte, An enhanced progressive damage model for laminated fiber-reinforced composites using the 3D hashin failure criterion: A multi-level analysis and validation, Materials 17 (21) (2024).
[39] X. Xu, M.R. Wisnom, X. Li, S.R. Hallett, A numerical investigation into size effects in centre-notched quasi-isotropic carbon/epoxy laminates, Compos. Sci. Technol. 111 (2015) 32–39.
[40] N. Zobeiry, R. Vaziri, A. Poursartip, Characterization of strain-softening behavior and failure mechanisms of composites under tension and compression, Compos. Part A: Appl. Sci. Manuf. 68 (2015) 29–41.
[41] I. Kaleel, E. Carrera, M. Petrolo, Progressive delamination of laminated composites via 1D models, Compos. Struct. 235 (2020).